Measuring vertical soil water content profiles by combining horizontal borehole and dispersive surface ground penetrating radar data

Yi Yu*, Anja Klotzsche, Lutz Weihermüller, Johan Alexander Huisman, Jan Vanderborght, Harry Vereecken and Jan van der Kruk

Agrosphere (IBG-3), Institute of Bio- and Geosciences, Forschungszentrum Jülich GmbH, Jülich, 52425, Germany

ABSTRACT

To investigate transient dynamics of soil water redistribution during infiltration, we conducted horizontal borehole and surface ground penetrating radar measurements during a 4-day infiltration experiment at the rhizontron facility in Selhausen, Germany. Zero-offset ground penetrating radar profiling in horizontal boreholes was used to obtain soil water content information at specific depths (0.2, 0.4, 0.6, 0.8 and 1.2 m). However, horizontal borehole ground penetrating radar measurements do not provide accurate soil water content estimates of the top soil (0–0.1 m depth) because of interference between direct and critically refracted waves. Therefore, surface ground penetrating radar data were additionally acquired to estimate soil water content of the top soil. Due to the generation of electromagnetic waveguides in the top soil caused by infiltration, a strong dispersion in the ground penetrating radar data was observed in 500 MHz surface ground penetrating radar data. A dispersion inversion was thus performed with these surface ground penetrating radar data to obtain soil water content information for the top 0.1 m of the soil. By combining the complementary borehole and surface ground penetrating radar data, vertical soil water content profiles were obtained, which were used to investigate vertical soil water redistribution. Reasonable consistency was found between the ground penetrating radar results and independent soil water content data derived from time domain reflectometry measurements. Because of the improved spatial representativeness of the ground penetrating radar measurements, the soil water content profiles obtained by ground penetrating radar better matched the known water storage changes during the infiltration experiment. It was concluded that the combined use of borehole and surface ground penetrating radar data convincingly revealed spatiotemporal soil water content variation during infiltration. In addition, this setup allowed a better quantification of water storage, which is a prerequisite for future applications, where, for example, the soil hydraulic properties will be estimated from ground penetrating radar data.

Key words: Ground-penetrating radar, Hydrogeophysics, Data processing.

INTRODUCTION

Characterizing soil water content (SWC) dynamics in unsaturated soil is important for a range of applications, including monitoring of pollutant transport (e.g. Binley *et al.*, 2001),

*E-mail: y.yu@fz-juelich.de

investigating root and plant growth processes (e.g. Cai *et al.*, 2018a) and estimating subsurface hydrogeological properties (e.g. Knight, 2001). Ground penetrating radar (GPR) is a popular hydrogeophysical method to investigate SWC dynamics because of its potentially high spatial resolution (Huisman *et al.*, 2003a; Slob, Sato and Olhoeft, 2010; Binley *et al.*, 2015) and the direct relationship between SWC and dielectric permittivity, which in turn determines the propagation of electromagnetic waves between GPR antennae. Over the last years, GPR has been widely used for investigating spatial SWC variability, monitoring SWC variations and estimating soil hydraulic properties (e.g. van Overmeeren, Sariowan and Gehrels, 1997; Huisman *et al.*, 2001, 2002; Redman, Parkin and Annan, 2000; Galagedara *et al.*, 2002; Jadoon *et al.*, 2012 Pan *et al.*, 2012; Steelman, Endres and Jones, 2012; Busch *et al.*, 2013; Allroggen, van Schaik and Tronicke, 2015; Iwasaki *et al.*, 2016; Jaumann and Roth, 2018; Klotzsche *et al.*, 2018).

GPR measurements can be conducted by using antennae placed at the surface or in boreholes. Surface GPR measurements have been used to obtain high-resolution SWC information using different acquisition strategies. A range of studies have shown that the ground wave that travels directly from the transmitter to the receiver through the top soil has potential for spatial mapping of SWC (Huisman *et al.*, 2003b; Galagedara *et al.*, 2005a; Weihermüller *et al.*, 2007). Due to the unclear penetration depth of the ground wave (Galagedara, Parkin and Redman, 2005b; Grote *et al.*, 2010), it is, however, not possible to determine vertical SWC profiles from this type of GPR measurements. Multi-offset reflection methods have also been used to estimate SWC in both field-scale (Lunt, Hubbard and Rubin, 2005) and lab-scale studies on SWC dynamics (Mangel *et al.*, 2012). However, the energy of reflected waves is often relatively weak and can thus be easily distorted by other radiated energy, which may lead to biased SWC estimates, especially in the case of heterogeneous permittivity distributions commonly associated with infiltration events. In addition, there is only limited control on the vertical resolution of SWC measurements obtained with the reflection method, because it depends on the position of the reflectors in the soil (Huisman *et al.*, 2003b). Therefore, conventional ground wave and reflection methods are not well suited to obtain high-resolution vertical SWC profiles by using GPR.

Borehole GPR can provide high-resolution geophysical information of the shallow subsurface, and this approach has been used to characterize soil properties for many years (e.g. Holliger, Musil and Maurer, 2001; Doetsch *et al.*, 2010;

Dafflon, Irving and Barrash, 2011; Klotzsche *et al.*, 2013; Yang *et al.*, 2013). Zero-offset profiling (ZOP) is a widely used acquisition strategy for borehole GPR measurements (e.g. Rejiba *et al.*, 2011), in which the transmitting and receiving antenna are moved simultaneously with a fixed step size in two different boreholes. Standard ray-based analysis methods can then be used to obtain a one-dimensional velocity profile between the two boreholes. Recently, several time-lapse plot-scale studies focused on SWC variation using horizontal borehole GPR measurements at specific depths, which ensures a good control on the vertical resolution of the obtained SWC profile information (Cai *et al.*, 2016; Klotzsche *et al.*, 2019). These studies mainly investigated seasonal SWC variations for different soils, surface treatments and the influence of plant types. It was found that the horizontal borehole GPR measurements did not provide accurate information close to the soil surface (0–10 cm) because of interference between the critically refracted airwave and the direct wave (Klotzsche *et al.*, 2019). This is obviously problematic when investigating infiltration processes, because the top soil is the most dynamic area with the strongest SWC changes. One possibility to overcome this limitation is to combine horizontal borehole and surface GPR measurements.

It has been observed that increased near-surface SWC associated with infiltration leads to low-velocity waveguides (van der Kruk, Streich and Green, 2006). In such waveguides, total reflection of the GPR waves occurs on the boundary between the wet and dry soil, which generates a guided wave through the constructive interference of the critical reflections and the ground wave causing late-arrival high-amplitude events in the data (Arcone, Peapples and Liu, 2003). Such guided waves show a pronounced dispersion in multi-offset surface GPR data, and thus a frequency-dependent velocity where phase velocities are different from the group velocity (van der Kruk *et al.*, 2009). Dedicated analysis methods are required to obtain relevant information from guided waves. In a first step, a phase velocity spectrum is calculated (Park, Miller and Xia, 1998) and the strongest energy in the spectrum is used to determine the phase velocity of different frequencies. With this frequency-dependent phase velocity, single-layer (van der Kruk *et al.*, 2006), multi-layer (van der Kruk, Jacob and Vereecken, 2010) or piece-wise linear models (Mangel, Moysey and van der Kruk, 2015) can be used to determine waveguide properties (e.g. permittivity, layer thickness) using model inversion. For example, single-layer waveguide inversion has been used to obtain the average dielectric permittivity and thickness of the waveguide during infiltration (Cassiani *et al.*, 2009; Rossi *et al.*, 2015). Using a piece-wise linear

model in the waveguide inversion, it is also possible to obtain a continuous and smooth SWC profile that may be more appropriate to describe the actual vertical distribution of SWC during and after infiltration events (Mangel *et al.*, 2017).

Until now, no study has been conducted that combines surface GPR with horizontal borehole GPR to study soil water content changes. Therefore, the aim of this study is to evaluate the accuracy and consistency of combined surface and horizontal borehole GPR results obtained during a dynamic infiltration experiment. In order to achieve this aim, transient SWC changes up to a depth of 1.2 m were monitored during a well-controlled infiltration experiment using ZOP surveys in horizontal boreholes. In addition, surface GPR measurements were conducted to characterize infiltration-induced waveguides in order to obtain SWC of the upper 0.1 m of soil. As a reference for the GPR results, TDR measurements were recorded at the same depths of the horizontal boreholes during the infiltration experiment. To assess the accuracy of the GPR and TDR results, the measured increase in water storage of these two methods was compared with the known irrigation amount used in the infiltration experiment.

MATERIALS AND METHODS

Infiltration experiment

The infiltration experiment was performed at the upper terrace minirhizotron facility in Selhausen, Germany (Cai *et al.*, 2016; Kelter *et al.*, 2018). The facility is divided into three plots (3 × 7 m) with different water treatments (natural rain, rain-out shelter and irrigated). Horizontal rhizotubes and soil sensors can be accessed via an access trench on one side of the facility (Fig. 1). Rhizotubes of 7 m length were installed at 0.1, 0.2. 0.4, 0.6, 0.8 and 1.2 m depths across the field with a horizontal offset of 0.1 m between tubes at different depth levels (see Fig. 1d). Here, it has to be noted, that the installation of the boreholes was done after excavating the entire plot up to a depth of 1.5 m as undisturbed installation of the boreholes using a drilling device into the stony native soil was not feasible. After excavation, the soil was refilled layer-wise and the boreholes (and other sensors) were installed during this backfilling. After completion of the facility, horizontal borehole GPR measurement could be carried out from the access trench by putting transmitter and receiver antennas into two neighbouring (rhizo-) tubes at the same depth (Fig. 1b).

Time domain reflectometry (TDR) measurements were made hourly by using a TDR100 system connected to a CR3000 data logger (both Campbell Scientific, Logan, USA) and the 50C81-SDM multiplexer as described by Weihermüller *et al.* (2013). Custom-made three-rod TDR sensors with a rod length of 200 mm and a spacing of 26 mm were installed 0.75 m away from the facility wall into the soil at the same depths as the tubes used for ground penetrating radar (GPR) measurements. Stones and gravel larger than 60 mm were removed around the location of the TDR sensors during installation. For more details on the construction of the minirhizotron facility and the installed sensors, we refer to Cai *et al.* (2016).

The infiltration experiment was conducted in the sheltered plot (Fig. 1a) using a drip irrigation system (Fig. 1c). The plot was completely sheltered several weeks before the start of the experiment to ensure dry initial soil conditions. The distance between two neighbouring dripping tubes was 0.30 m, and the distance between the drippers was 0.20 m. To ensure irrigation at a constant rate, water was first poured into an underground water tank and then pumped out from that to supply the drip irrigation system. The water volume was recorded by a flow meter between the water pump and the drip irrigation system.

Five infiltration events were performed between the 30 September 2013 and the 3 October 2013 (Table 1). Horizontal borehole and surface GPR measurements were taken using a PulseEKKO system (Sensors & Software, Canada) during the first 4 days of the infiltration experiment. For the borehole measurements we used 200 MHz dipole antennae, and for the surface measurements we used unshielded 100 and 200 MHz as well as shielded 500 MHz antennae.

Although the saturated hydraulic conductivity ($K_s = 34$ mm/hour; Cai *et al.*, 2018b) of the topsoil is much larger than the average irrigation rate (18 mm/hour), ponding at the soil surface was observed on the first day of the experiment. Ponding was not observed anymore during the following infiltration events. Before, during and after the daily infiltration events, ZOP GPR measurements were performed in the horizontal borehole pairs. As the soil water content (SWC) is assumed to increase mainly at shallow depths at the beginning of each consecutive infiltration event, only the horizontal boreholes at 0.2 and 0.4 m depth were measured during the infiltration event to ensure that all measurements could be performed within the irrigation interval. After the irrigation stopped, the deeper boreholes were also measured. Additionally, more than 140 wide angle reflection and refraction (WARR) measurements were obtained with surface GPR during the infiltration experiment (see Fig. 1c for setup).
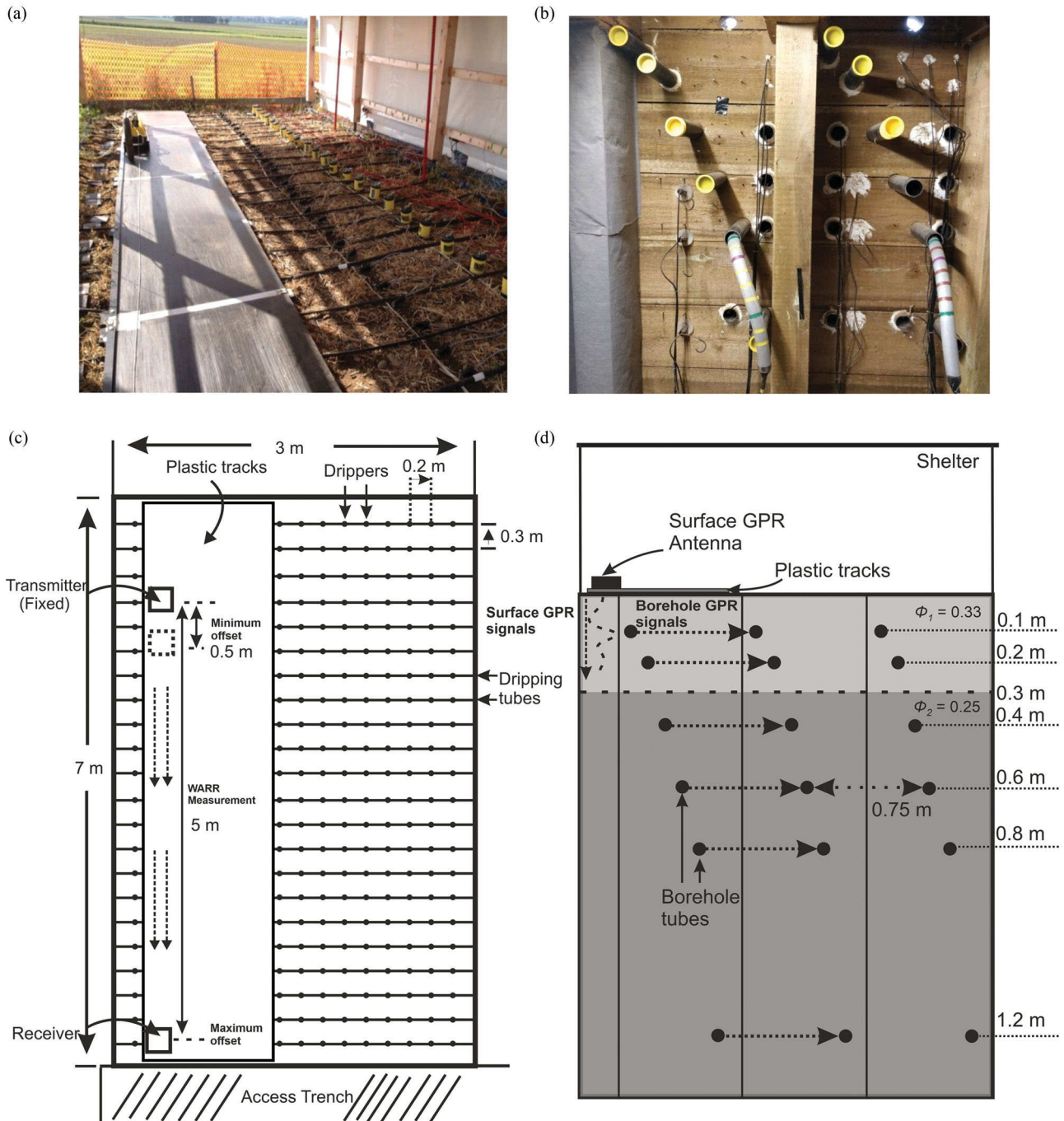
Figure 1 (a) Photograph of the setup of the infiltration experiment (surface) and (b) horizontal boreholes used for GPR measurements and location of the TDR sensors. (c) schematic setup of the drip irrigation system at the soil surface and (d) sketch of the entire acquisition set-up with surface GPR and horizontal borehole tubes.

Horizontal borehole ground penetrating radar data acquisition and processing

For the zero-offset profiling (ZOP) measurements, we followed the same acquisition, processing and analysis strate-

gies as presented in Klotzsche *et al.* (2019). To conduct the ZOP survey, the transmitter (*Tx*) and receiver (*Rx*) antenna were first pushed to the end of the horizontal boreholes (7 m) at the same depth. Then, both antennae were pulled

Table 1 Overview of infiltration events during the experiment

Date	Start Time	End Time	Water Volume (L/m^2)	T (°C)	EC (μS/cm)
30/09/2013	14:54	16:24	28.4	17.0	513
01/10/2013	12:24	13:54	27.3	17.0	513
02/10/2013	12:45	14:15	28.0	16.0	500
03/10/2013	12:24	13:54	26.1	14.4	488
03/10/2013	14:28	15:58	27.0	14.4	488

simultaneously in 0.05 m steps towards the access trench wall up to a minimum distance of 1.5 m to the wall. Using the recorded arrival time (t) and the known distance between the two boreholes ($d = 0.75$ m), the velocity of the radar wave (v) can be determined using

$$v = \frac{d}{t - T_0}, \tag{1}$$

where T_0 is the so-called time-zero offset (Fig. 2a). The determination of T_0 is difficult for borehole GPR measurements because no airwave is present, as is the case for surface GPR measurements. Therefore, T_0 was determined from multi-offset measurements with the borehole antennae in air (hereafter referred to as calibration WARR measurements). An accurate determination of T_0 is important because the pulse onset time can drift during the GPR survey and relatively small changes in T_0 can easily introduce substantial velocity changes and thus erroneous SWC estimates (Peterson, 2001), in particular in the case of the small borehole separations used here. In order to determine T_0, the following procedure was used. In a first step, the first maximum and zero crossing of each trace in the calibration WARR measurement (inset of Fig. 2b) is determined automatically. Then, a constant time difference between the actually needed first arrival time and first zero crossing is determined for a certain number of traces by manual time picking. This constant time offset is different for the calibration measurement and the ZOP data due to the different centre frequencies. The first arrival of each GPR trace is then obtained by subtracting the constant time difference from the zero-crossing times for all traces. Finally, T_0 is determined as the intercept of a line with a fixed slope (1/0.3 m/ns) fitted to the first arrival times. In order to account for drifts in T_0, calibration WARR measurements were made regularly in between ZOP measurements. Some drift in T_0 as a function of time was observed, and the most appropriate value for T_0 at the time of each ZOP measurement was determined by linear interpolation between calibration measurements. After the determination of v for each ZOP measurement using equa-

tion (1), the dielectric permittivity (ε) at different depths was obtained by

$$\varepsilon = \left(\frac{c}{v}\right)^2, \tag{2}$$

where c is the speed of light in vacuum (299,792,458 m/s).

Surface ground penetrating radar data acquisition and processing

Surface GPR measurements were made on a plastic track to prevent contact between the antenna and the irrigation water as well as to protect the soil from being damaged by the operators of the surface GPR system. The offset range of the surface WARR measurement was from 0.5 to 5.0 m (see Table 2 for acquisition parameters). First, the T_0 of the data surface GPR data is calibrated as the intercept of a line that determined by a fixed slope (1/0.3 m/ns) and the picked first arrival time of airwave at 0.5 m offset. A combined linear move-out (LMO) and hyperbolic move-out (HMO) semblance analysis approach (Dal Bo *et al.*, 2019) was used to analyse the 100 and 200 MHz data. These GPR measurements did not show velocity dispersion associated with infiltration because the wavelength at these frequencies is much larger than the thickness of the wetted top soil layer. The velocity of the direct ground wave was extracted by LMO. HMO was used to estimate the velocity of the reflected wave. An empirical function (van Overmeeren *et al.*, 1997; Grote, Hubbard and Rubin, 2003) was employed to estimate the sampling depth (z) of the ground wave:

$$z = \frac{1}{2}\sqrt{\frac{v_{Gw}S}{f}}, \tag{3}$$

where v_{Gw} is the velocity of the ground wave, S is the distance between transmitter and receiver and f is the centre frequency of the antenna. Based on this relationship, it can be seen that sampling depth decreases with increasing frequency and SWC (Grote *et al.*, 2010).

After the first infiltration event, the WARR measurements made with the 500-MHz antenna showed dispersive
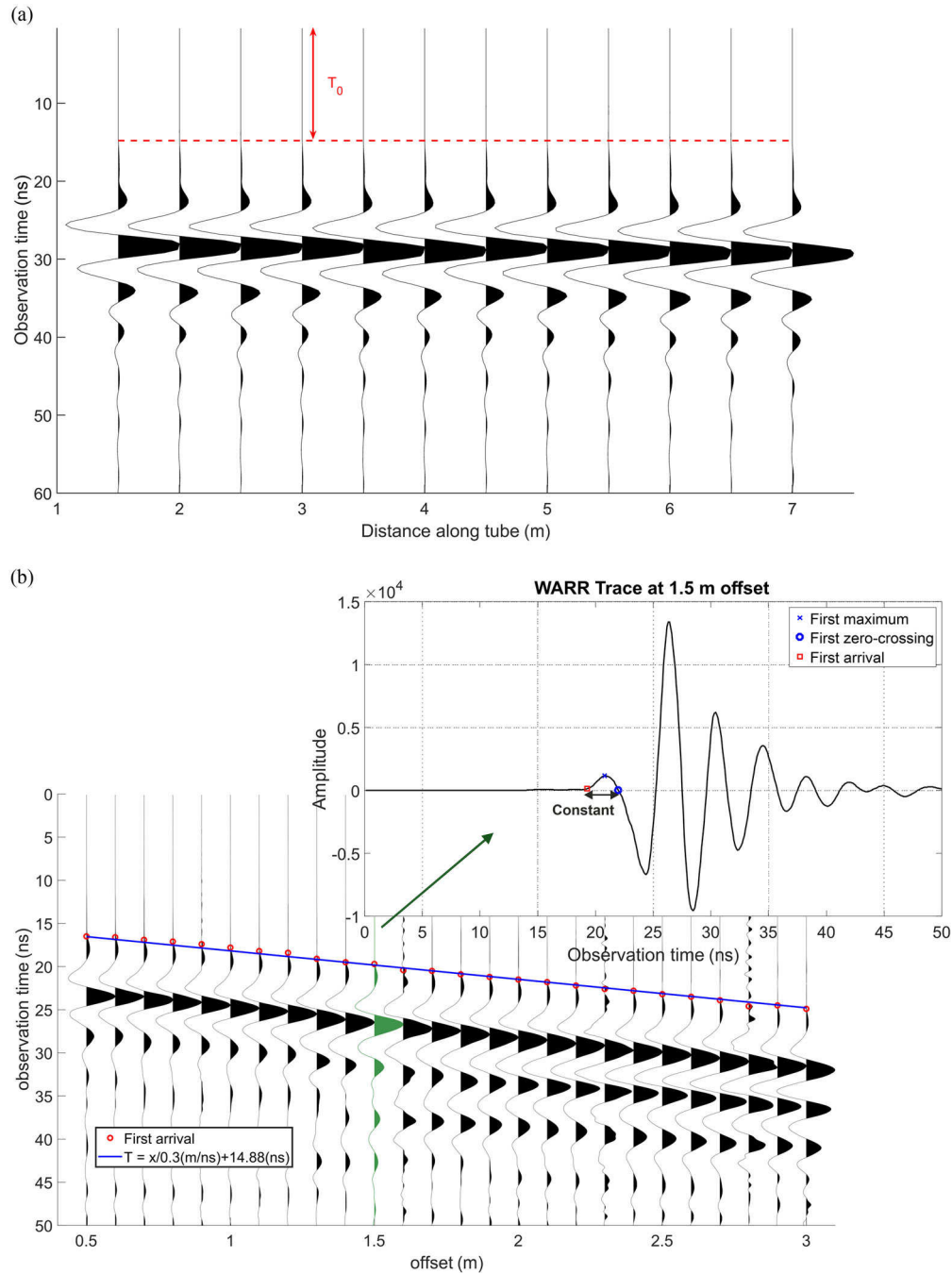
(a)

(b)

Figure 2 (a) Typical 200 MHz ZOP data for horizontal borehole GPR. The appropriate T_0 is determined from a WARR measurement in air. (b) Illustration of T_0 estimation from a WARR measurement with 200 MHz antenna. The first arrival time of all traces are indicated by red dots. T_0 is the intercept of the regression line for the first arrival of the airwave as a function of antenna offset (blue line). The inset illustrates the determination of the time difference between the first arrival (red dot) and the first zero-crossing (blue dot).

waves. The following procedure was used to process these dispersive data. In a first step, the airwave was muted and the guided wave (Fig. 3a) was selected to generate a phase-velocity spectrum (Fig. 3c and 3d). Next, the phase velocity

for different frequencies ($v_{data}(f_i)$) was obtained by picking the maximum energy for each frequency in the phase velocity spectrum (black line, Fig. 3d). The centre frequency of the measured data (350 MHz, Fig. 3b) is commonly less than that

Table 2 Overview of data acquisition of surface GPR

Frequency (MHz)	Sampling Interval (m)	Time Window (ns)	Sampling Rate (ns)	Stack
100	0.05	100	0.4	32
200	0.05	200	0.4	32
500	0.01	50	0.2	32

of the GPR antenna (500 MHz), and it can be observed from the amplitude spectrum (Fig. 3b) that the effective bandwidth is approximately between 200 and 700 MHz when using a threshold of 15% of the maximum amplitude. This bandwidth is used in the following analysis of the frequency-dependent phase velocity.

Surface ground penetrating radar data acquisition and processing

Single-layer low-velocity waveguide inversion was employed to invert the dispersive surface GPR data to obtain the thickness (h), average permittivity of the wet layer (ε_1), and the underlying material (ε_2). For this, the theoretical phase velocity ($v_{model}(f_i, \varepsilon_1, \varepsilon_2, h)$) was calculated by solving the equation established by the given waveguide parameters ($\varepsilon_1, \varepsilon_2, h$):

$$v_{model}(f_i, \varepsilon_1, \varepsilon_2, h) = \frac{c}{\sqrt{\varepsilon_1} \sin[\theta(f_i, \varepsilon_1, \varepsilon_2, h)]}, \quad (4)$$

where $\theta(f_i, \varepsilon_1, \varepsilon_2, h)$ is the fundamental equation of modal theory (Arcone, 1984). Since the surface GPR measurements were conducted in the transverse electric (TE) mode, the fundamental modes (TE_0) and higher modes (TE_1, TE_2, etc.) of the guided wave can be present in the data, if the signals contain frequencies above the respective cut-off frequency (van der Kruk, 2006). The dispersion inversion of fundamental mode and higher modes was performed through minimization of a cost function ($C_m(\varepsilon_1, \varepsilon_2, h)$) based on the absolute
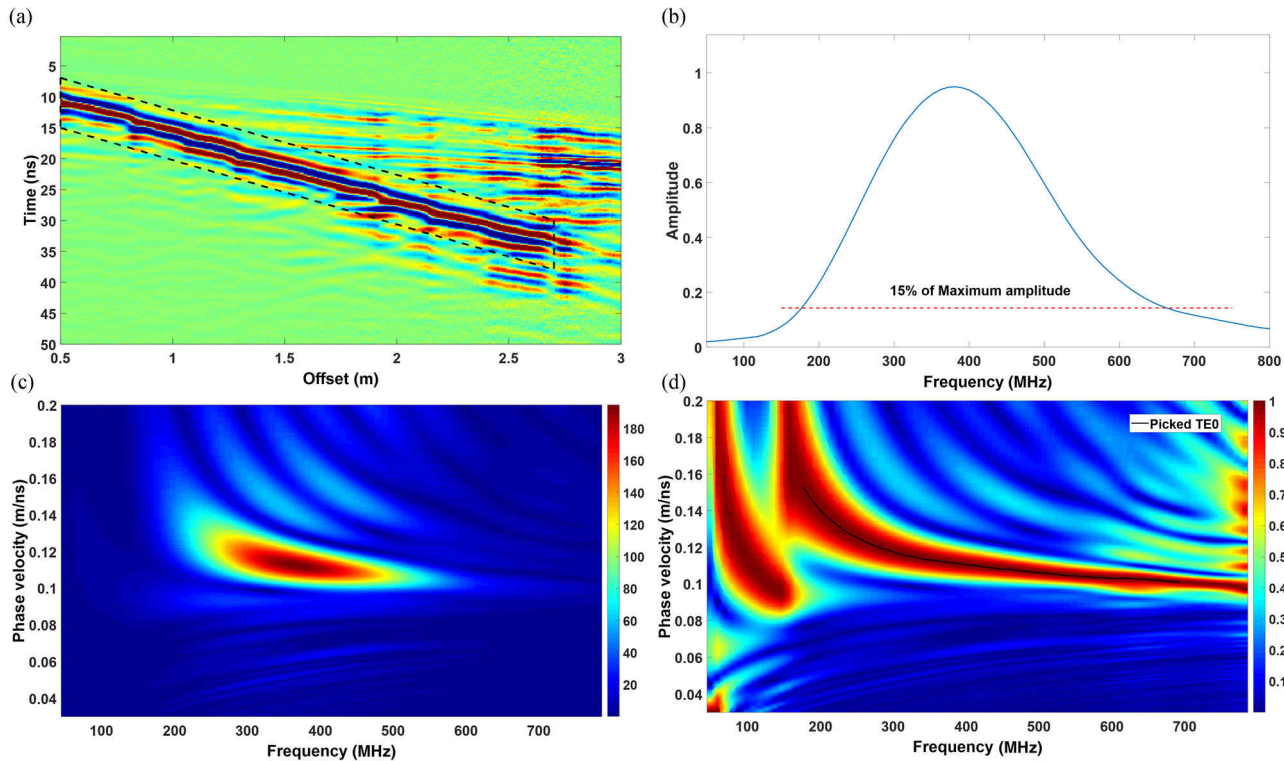

Figure 3 (a) Dispersive surface GPR dataset acquired at the end of the first infiltration event using 500 MHz antenna. Dashed lines indicated the zone used for the dispersion analysis. (b) Average frequency spectrum (normalized) of the GPR data. (c) Phase velocity spectrum before and (d) after normalization.

difference between $v_{\text{model}}^{\text{TE}_m}(f_i, \varepsilon_1, \varepsilon_2, h)$ and $v_{\text{data}}^{\text{TE}_m}(f_i)$ (van der Kruk *et al.*, 2006):

$$C_m(\varepsilon_1, \varepsilon_2, h) = \sum_{i=1}^{n} \frac{\left| v_{\text{data}}^{\text{TE}_m}(f_i) - v_{\text{model}}^{\text{TE}_m}(f_i, \varepsilon_1, \varepsilon_2, h) \right|}{n}, \quad (5)$$

where n refers to the number of frequency points picked in the phase velocity spectrum and m represents the mode of the guided wave. The inversion for single-layer waveguide parameters is very sensitive to ε_1 and partly to h (Strobbia and Cassiani, 2007), whereas the inverted ε_2 are typically not accurate. The uncertainty in the inversion of ε_2 is caused by simplifying the vertical SWC distribution to a single-layer waveguide and the stronger measurement noise in the low-frequency part of the phase velocity spectrum (below 200 MHz) (Bikowski *et al.*, 2012).

Determination of soil water content and storage

The complex refractive index model (Roth *et al.*, 1990) was used to relate the dielectric permittivity obtained with GPR and TDR to SWC according to the following equation:

$$\text{SWC} = \frac{\sqrt{\varepsilon} - (1 - \Phi)\sqrt{\varepsilon_s} - \Phi}{\sqrt{\varepsilon_w} - 1}, \quad (6)$$

where ε is the relative bulk permittivity. ε_w refers to the permittivity of water (84 at 10°C). The permittivity of the soil ε_s was considered to be 4.7 for this test site. It is important to notice that porosity Φ changed from 0.33 to 0.25 (cm³/cm³) at 0.3 m depth due to the presence of a plowing horizon (Fig. 1).

To verify the accuracy of the SWC estimates obtained by GPR and TDR, cumulative water storage (m) was calculated by integrating the measured SWC over the entire profile depth. The increase in water storage was then compared with the known irrigation amounts (Table 1). In the integration, it was assumed that the surface GPR measurements and the TDR measurements at 0.1 m depth represent the average SWC of the 0–0.1 m depth range. Furthermore, the horizontal borehole GPR and TDR measurements at 0.2, 0.4, 0.6, 0.8 and 1.2 m depth were assumed to represent the mean SWC of 0.1–0.3, 0.3–0.5, 0.5–0.7, 0.7–0.9 and 0.9–1.3 m depth, respectively. The water storage was also calculated from the borehole GPR measurements only. Here, it was assumed that the GPR measurements at 0.2 m depth were representative for the mean SWC of the top 0.30 m of soil.

RESULTS AND DISCUSSION

Horizontal borehole ground penetrating radar data

For a reliable estimation of the soil water content (SWC) changes due to infiltration, the time zero T_0 has to be known accurately. The change in T_0 during the infiltration experiment is shown in Fig. 4. The maximum difference between two adjacent T_0 estimates was relatively small on day 1 (0.34 ns) and day 2 (0.73 ns), but was larger on day 3 (0.96 ns) and day 4 (0.8 ns). The largest variation of T_0 occurred on day 3, which could be caused by a too short warm-up period of the ground penetrating radar (GPR) system on
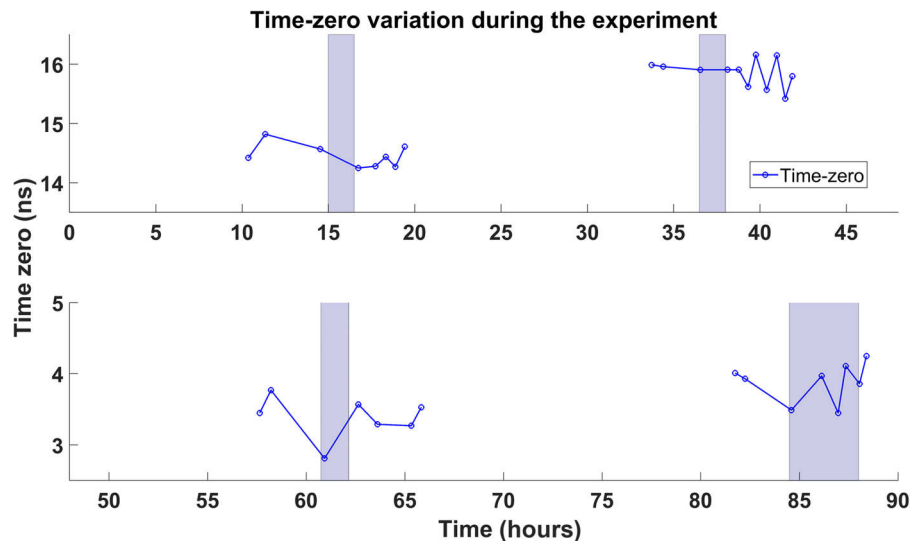

Figure 4 The time-zero T_0 variation during the entire experiment. The duration of the infiltration events is indicated by the light blue background. Note that the *y*-axis has different scales for the first 2 and last 2 irrigation events.
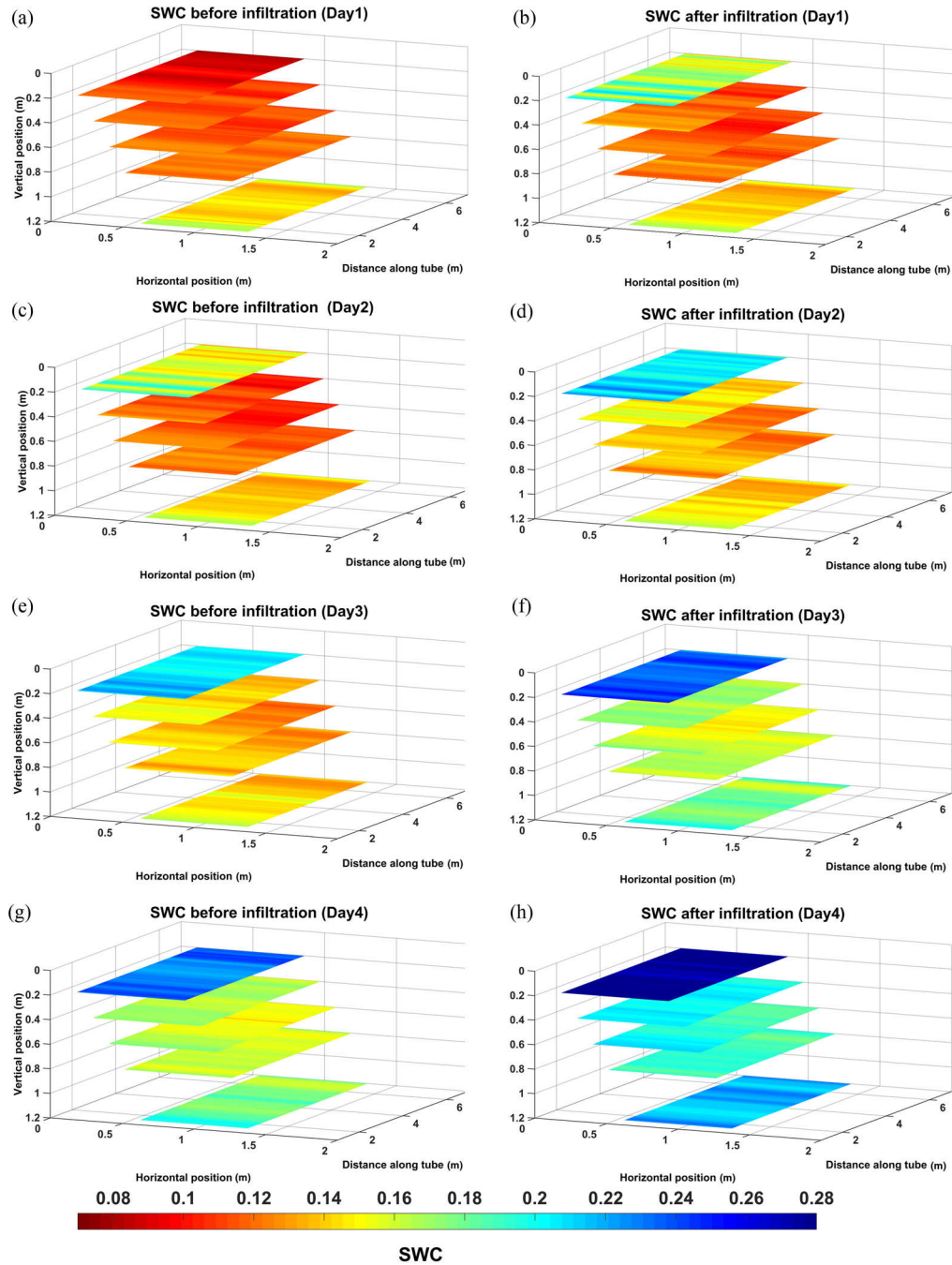
Figure 5 Semi-three-dimensional image of SWC estimates from horizontal borehole GPR. Panels on the left side (a, c, e and g) were measured before infiltration events for the four respective days, whereas panels on the right side (b, d, f and h) were measured after the infiltration events for the respective days.

this day. The uncertainty in the SWC estimates resulting from a 0.96-ns time-shift is 0.047 cm³/cm³ independent of the SWC.

Spatial SWC variation along the horizontal borehole tubes at five depths before and after the four infiltration events

are shown in Fig. 5. Before the start of the infiltration experiment, the deeper soil was generally wetter than the top soil (Fig. 5a). After the infiltration event on day 1, an increase of the SWC was mainly observed at 0.2 m depth and the deeper
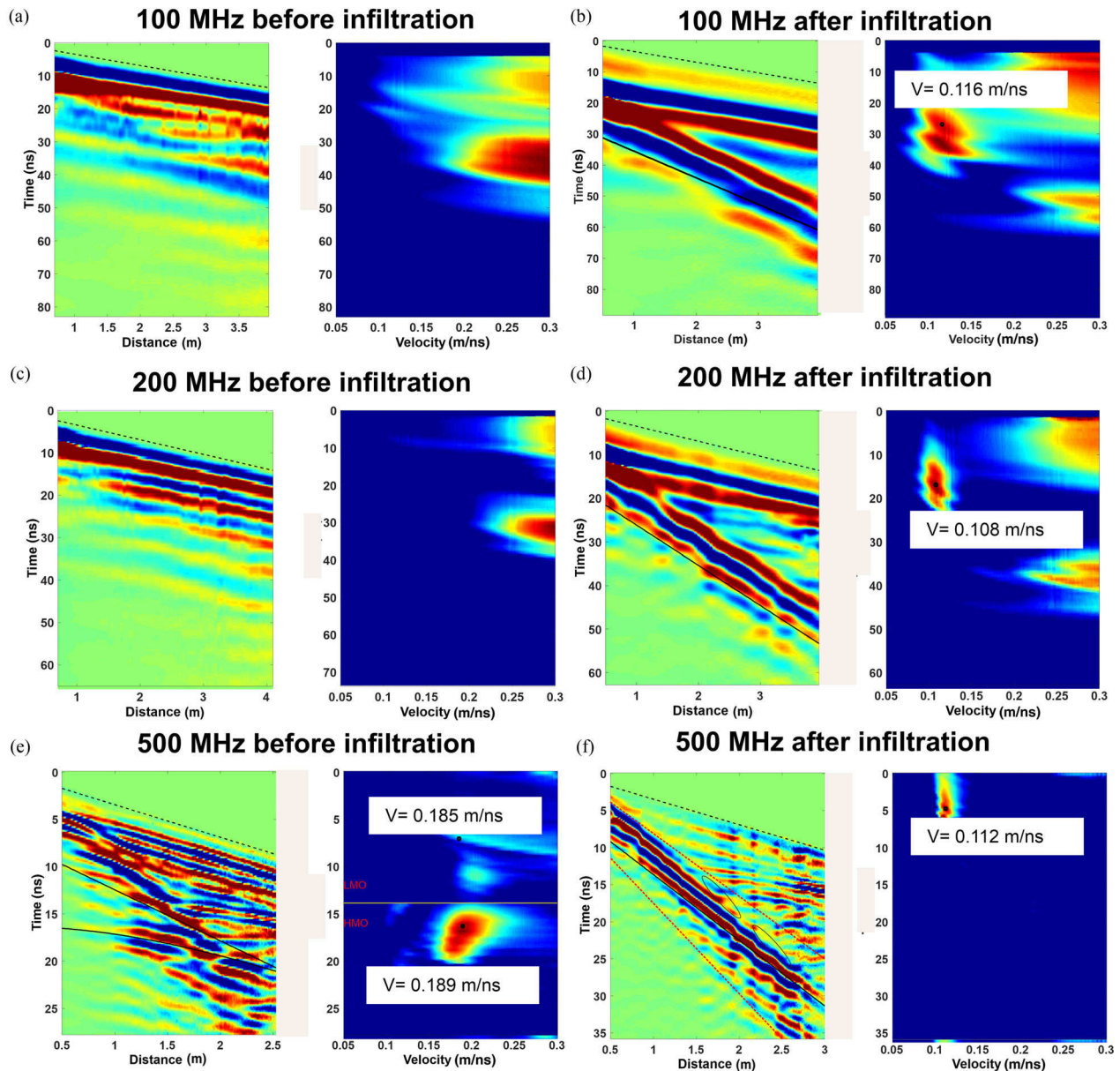
Figure 6 WARR measurements with 100, 200 and 500 MHz data before (right panel a, c, e) and (left panel b, d, f) after infiltration and their semblance spectra. The black dashed lines indicate the first arrival of the direct airwave. The guided wave is enclosed by red dashed lines. The velocities of the ground and reflected wave were picked in the semblance spectra and indicated by the black circles. The corresponding ground and reflected waves are shown by straight and hyperbolic lines in the WARR measurements, respectively. The phase shift of guided wave is enclosed by the eclipses.

soil was less affected. Moreover, infiltration introduced lateral heterogeneity in SWC at 0.2 m depth, especially at the first and second day, which could be caused by the layout of the dripping system and the heterogeneity of the soil. During the infiltration events at day 3 and 4, the soil at 0.2 m depth was almost saturated and an increase of SWC was observed at all depths.

Semblance analysis of surface ground penetrating radar data

The results of the semblance analysis for three different frequencies before and after infiltration are exemplary shown in Fig. 6. For the 100 and 200 MHz measurements gathered before infiltration (Fig. 6a,c), only the airwave could be identified because the soil was very dry and a large part of the
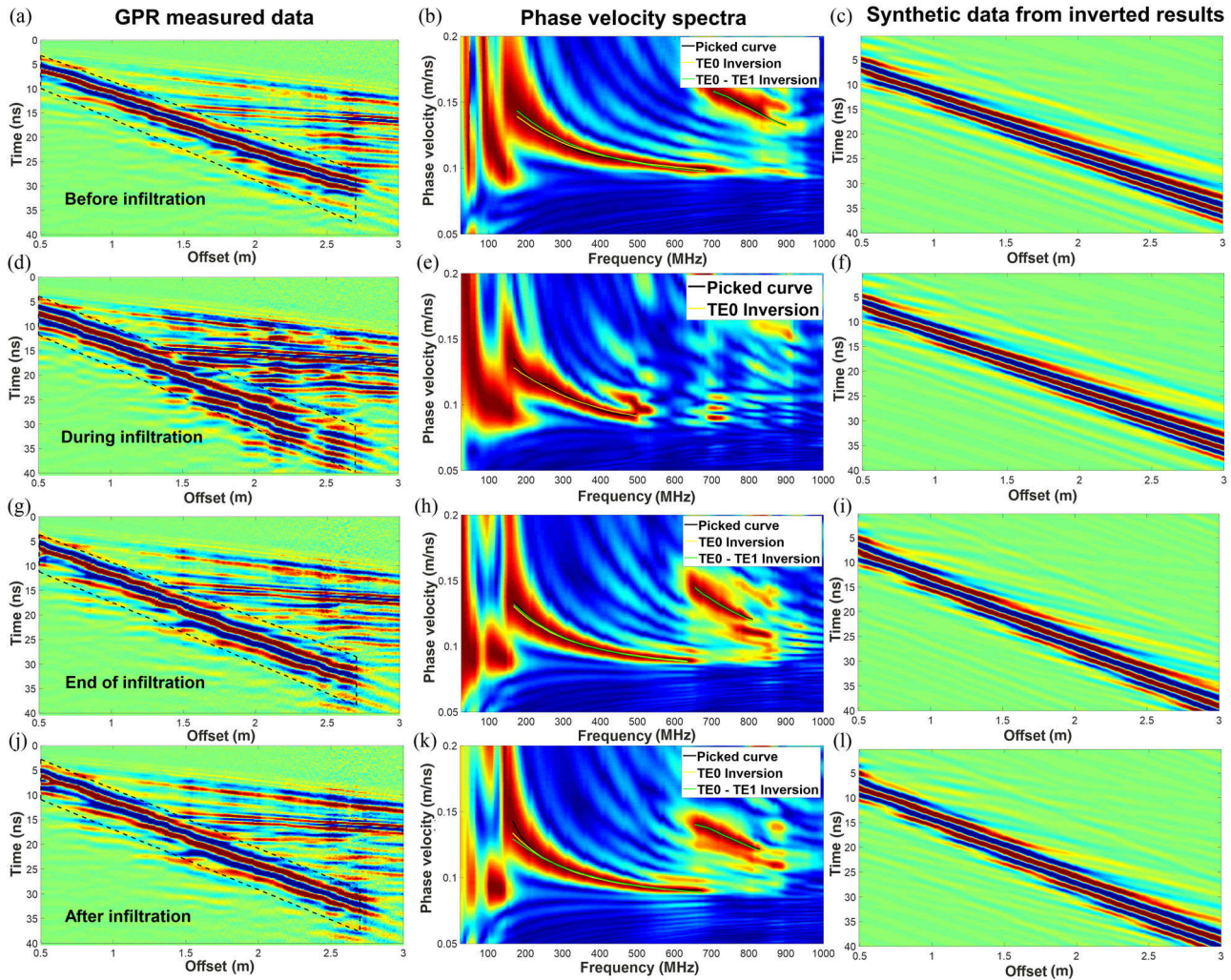
Figure 7 Four typical dispersive WARR measurements with associated phase velocity spectra and modelled WARR measured obtained (a, b, c) before, (d, e, f) at the start of the infiltration event, (g, h, i) at the end of the infiltration event and (j, k, l) after the infiltration event on day 2 of infiltration experiment. The guided waves are enclosed by the black dashed lines (left panel), which were also used to generate corresponding phase-velocity spectra. Synthetic modelled WARR data based on the TE_0 inversion results.

radiation energy was thus contained in this wave. For the 500-MHz data (Fig. 6e), a reflection from the bottom of the excavated field plot is observed as a hyperbolic move-out. Because of the strong interference with the airwave, the estimated velocity (0.19 m/ns) from the semblance analysis is not accurate and can therefore not be used to estimate SWC. After infiltration, a clear ground wave could be observed for all frequencies (Fig. 6b,d,f). Additionally, the phase shift of the ground wave in Fig. 6(f) suggests that the 500-MHz data were dispersive after the infiltration event, which was not observed in the 100 and 200 MHz data.

Dispersion analysis of surface ground penetrating radar data

After the infiltration event of day 1, a dispersive ground wave was observed during the remainder of the infiltration experiment. Four typical wide angle reflection and refraction (WARR) measurements obtained at day 2 of the infiltration experiment are shown in Fig. 7. The first WARR measurement (Fig. 7a) was obtained before the start of the infiltration on day 2. The low-velocity waveguide induced by the irrigation event of day 1 was still clearly present. The dispersion curve of the TE_0 is well defined and smooth, and the first higher mode TE_1 can also be easily identified (Fig. 7b).

Table 3 inversion results of day 2 using 500 MHz dispersive data

Data	Inversion methods	ε_1; SWC (cm^3/cm^3)	ε_2	H (m)	Cost function (m/ns)
Fig. 7a	TE$_0$	11.40; 0.201	3.82	0.100	0.0013
	TE$_0$-TE$_1$	12.25; 0.224	3.57	0.084	0.0019
Fig. 7d	TE$_0$	16.59; 0.294	4.88	0.068	0.0017
Fig. 7g	TE$_0$	14.22; 0.257	3.85	0.095	0.0007
	TE$_0$–TE$_1$	14.82; 0.266	3.75	0.087	0.0011
Fig. 7j	TE$_0$	13.94; 0.253	3.27	0.097	0.0009
	TE$_0$–TE$_1$	14.43; 0.261	4.54	0.085	0.0019

In a first step, the TE$_0$ mode was used for inversion (Table 3). To validate the obtained results of the dispersion inversion, we performed synthetic forward modeling with the obtained inversion results using the GprMax software (Giannopoulos, 2005; Warren, Giannopoulos and Giannakis, 2016) (Fig. 7c,f,i,l). The slope and the phase shift of the simulated guided waves matched well with the measured data. It should be mentioned that the field was relatively heterogeneous at the beginning of the infiltration due to the layout of the dripping system. Therefore, the dispersion curve of the data measured at the beginning of the infiltration event (Fig. 7e) was not only found to be distorted and of shorter frequency range (200–500 MHz) than other data, but also the TE$_1$ mode could not be identified. Consequently, a large ε_1 and a small layer thickness h were obtained with a larger uncertainty from inversion (Bikowski *et al.*, 2012).

In a second step, data for the TE$_0$ and TE$_1$ mode were jointly inverted (Table 3). Compared to the inversion with TE$_0$ only, the TE$_0$–TE$_1$ inversion generally resulted in slightly larger ε_1 and smaller layer thickness h. TE$_0$ and TE$_0$-TE$_1$ results showed a good consistency, and the largest difference between these two inversion approaches was also small with a difference of 0.085 for ε_1 and 0.016 m for h. Therefore, it was concluded that the consideration of the TE$_1$ mode in the inversion did not result in different waveguide parameters compared to the use of the TE$_0$ mode only. Additionally, since the TE$_1$ mode could not be identified for all measured GPR data, it was preferred to consistently use the TE$_0$ mode only for inversion.

The SWC estimates from the semblance and dispersion analysis as well as the calculated sampling depth derived from equation (3) are summarized in Table 4 for all surface GPR measurements. For the 500-MHz data, the SWC estimates obtained from semblance and dispersion analysis deviated considerably. This is due to the fact that the SWC obtained by semblance analysis is based on the group velocity of the guided wave, which is always lower than the phase velocity according

to equation (4). As a result, semblance analysis underestimated SWC of the top layer for 500 MHz measurements. The results of the dispersion analysis suggest that the thickness of the waveguide was around 0.1 m during the entire experiment. This is attributed to layering caused by regular agricultural activity.

Combined horizontal borehole and surface ground penetrating radar data

The SWC profiles obtained by combining the dispersion analysis and the mean SWC along the horizontal borehole tubes can be used to analyse the spatio-temporal soil water content evolution during the infiltration experiment (Fig. 8). As expected, changes in SWC were first observed at shallow depth (0.2 m) during the infiltration event on day 1. The GPR data gathered at 0.4 m depth also indicate a small increase in SWC, but measurements below 0.4 m were unaffected by the infiltrating water (Fig. 8a). Vertical SWC profiles measured before and after infiltration are shown in Fig. 9. After the irrigation event on day 1, the SWC obtained from surface GPR increased slightly overnight. This is possibly caused by the horizontal movement of water within the top soil layer during the night. After the start of the infiltration on day 2, the SWC increased and stayed at a relatively constant value and the thickness of the waveguide did not change. With further irrigation, the SWC close to the surface increased but water also moved downwards, as indicated by the increase in SWC below 0.4 m.

Water obviously redistributed to deeper depths between the infiltration event of day 2 and day 3 but also between day 3 and day 4 (Fig. 9). The SWC profiles for day 3 and day 4 show a clear increase in SWC for all depths during the infiltration event (Fig. 8c,d). The movement of the wetting front can clearly be seen in Fig. 9. After infiltration at day 1, the wetting front moved to a depth between 0.2 and 0.4 m. After the infiltration event at day 2, the upper 0.8 m depth
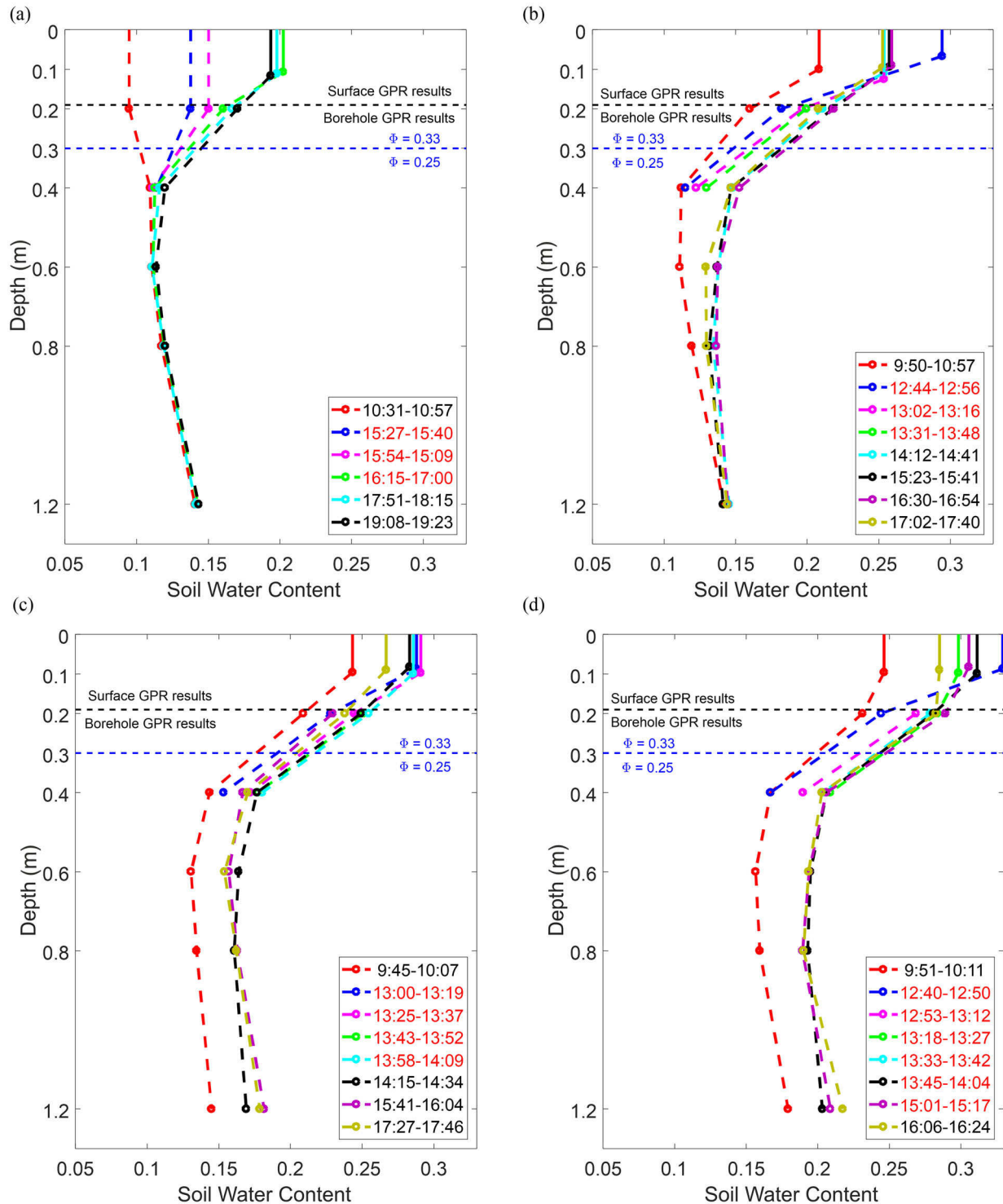
Figure 8 Vertical SWC profiles at (a) day 1, (b) day 2, (c) day 3 and (d) day 4. The colours indicate the different times when the measurements were performed, whereas measurements taken during infiltration are shown in red in the legend. Above the horizontal black dashed line, the surface GPR results are shown, whereas the averaged borehole GPR results are plotted below this line. Note that the total porosity Φ changes from 0.33 to 0.25 at 0.3 m depth as indicated by the blue solid line due to previous tillage practice.

Table 4 Results of semblance and dispersion analysis

| | Semblance Results SWC (cm³/cm³); sampling Depth z (m) | | | Dispersion Analysis (500 MHz) |
Time	100 MHz	200 MHz	500 MHz	SWC (cm³/cm³); h (m)
Day 1				
11:32	-	-	-	-
15:26[†]	0.125; 0.747	0.095; 0.554	0.075; 0.362	-
16:28	0.152; 0.718	0.116; 0.535	0.136; 0.328	0.202; 0.107
17:21	0.139; 0.731	0.119; 0.533	0.134; 0.329	0.189; 0.135
18:39	0.138; 0.732	0.125; 0.528	0.124; 0.330	0.198; 0.111
19:39	0.133; 0.738	0.129; 0.524	0.134; 0.329	0.194; 0.116
Day 2				
12:00	0.148; 0.722	0.137; 0.519	0.131; 0.330	0.201; 0.100
12:48[†]	0.173; 0.698	0.169; 0.495	0.163; 0.316	0.294; 0.068
13:41[†]	0.183; 0.688	0.182; 0.487	0.191; 0.304	0.254; 0.125
14:23[†]	0.178; 0.693	0.180; 0.488	0.171; 0.313	0.254; 0.108
15:53	0.179; 0.692	0.167; 0.497	0.168; 0.314	0.257; 0.095
17:04	0.168; 0.702	0.161; 0.501	0.167; 0.314	0.259; 0.090
18:02	0.173; 0.697	0.171; 0.495	0.155; 0.319	0.253; 0.097
Day 3				
10:50	0.179; 0.692	0.173; 0.493	0.153; 0.320	0.243; 0.096
13:09[†]	0.180; 0.691	0.186; 0.485	0.168; 0.314	0.289; 0.087
13:42[†]	0.204; 0.691	0.212; 0.469	0.191; 0.304	0.280; 0.097
14:22[†]	0.204; 0.691	0.197; 0.478	0.182; 0.308	0.286; 0.099
15:22	0.202; 0.672	0.189; 0.482	0.171; 0.313	0.283; 0.083
16:44	0.197; 0.676	0.188; 0.483	0.169; 0.314	0.269; 0.090
Day 4				
10:30	0.165; 0.705	0.179; 0.489	0.160; 0.317	0.247; 0.097
12:49[†]	0.185; 0.687	0.186; 0.484	0.173; 0.311	0.338; 0.062
13:21[†]	0.186; 0.686	0.210; 0.470	0.219; 0.294	0.298; 0.091
13:52[†]	0.197; 0.676	0.205; 0.473	0.189; 0.305	0.311; 0.082
15:07[†]	0.214; 0.663	0.204; 0.474	0.201; 0.300	0.306; 0.092
16:11	0.192; 0.680	0.215; 0.467	0.188; 0.306	0.285; 0.099

SWC is calculated by the CRIM.

The calculation of sampling depth of ground wave adopts the equation from van Overmeeren *et al.* (1997)

†Measuring times during the infiltration event.

were wetted but the SWC at 1.2 m depth did not change yet. For the infiltration events at day 3 and day 4, it was observed that SWC increased at all depths, which suggests that the wetting front quickly moved to below 1.2 m depth at these days, which is a consequence of the higher initial water content in the soil profile and the associated higher unsaturated hydraulic conductivity.

The time series of average SWC obtained with time domain reflectometry (TDR) sensors at six depths is shown in Fig. 10 along with the SWC estimated from the GPR measurements (average for the entire borehole length). It can be seen that the GPR and TDR measurements show a rapid and synchronous response to the four infiltration events, and sim-

ilar trends in SWC increase. Nevertheless, the SWC estimates obtained with GPR and TDR differed considerably, especially at 0.1 and 0.2 m depth. In particular, the SWC determined with GPR measurements was higher than the SW obtained with TDR measurements at 0.1 m and lower at 0.2 m depth. These differences are attributed to the different sensing volumes of the TDR and GPR measurements. The TDR sensors provide point measurements approximately 1 m away from the trench wall, whereas the GPR measurements represent the average SWC of the top soil from 1.5 to 7 m away from the trench. Therefore, GPR is expected to be more representative of the irrigated area and thus provide improved ability to monitor wetting front movement in this experiment. For
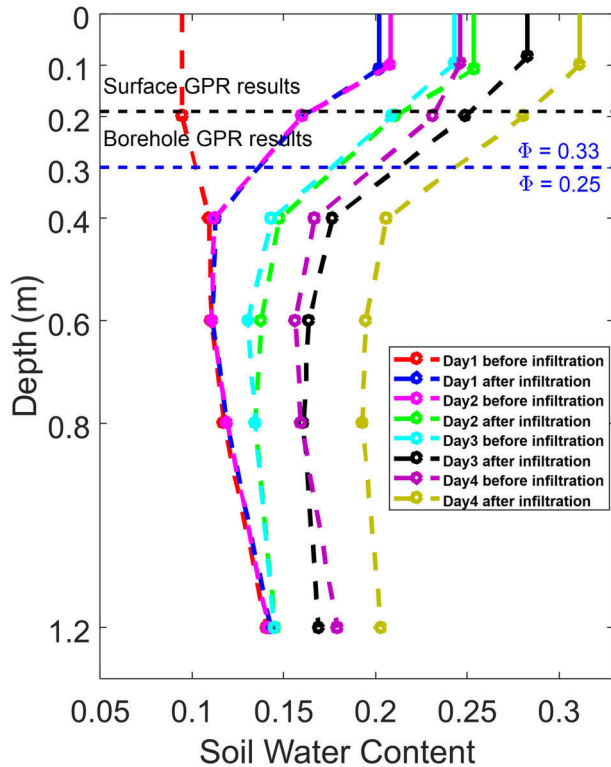
Figure 9 Combined GPR SWC profiles measured before and after infiltration events for all days.

example, SWC obtained with TDR increased up to a depth of 0.4 m during the first infiltration event, while the SWC obtained with GPR only responded at 0.1 and 0.2 m depth. Although it is possible that water infiltrated to 0.4 m depth in some places due to the spatial soil heterogeneity, it is unlikely that the wetting front moved to 0.4 m depth over the entire infiltration area because only 28.4 mm of water was applied in the first infiltration event.

The correlation between the depth-averaged SWC obtained with GPR and TDR is shown in Fig. 10(b). The linear regression between GPR and TDR results has a slope close to one, and the intercept is also small. This indicates an unbiased and fairly good agreement between GPR and the TDR data. However, there is substantial scatter in this relationship as indicated by the relatively low explained variance (R^2 of 0.63) and the high root mean square error (RMSE of 0.04 cm^3/cm^3). As mentioned before, the misfit is strongest for the shallow soil layers (0.1 and 0.2 m). There is a range of possible explanations for the relatively large misfit. First, there is some uncertainty in using surface GPR measurements to estimate SWC at 0.1 m depth since the inverted layer depth is varying around 0.1 m during the experiment and a homogeneous water content distribution in the top layer is assumed in the single-layer waveguide dispersion. Second, there is uncertainty in time-zero estimation for the horizontal borehole GPR data. Third, there is intrinsic uncertainty in the SWC estimates obtained with GPR and TDR. This includes uncertainty in travel time determination for both GPR and TDR and the uncertainty in the position of the horizontal boreholes. Fourth and foremost, there is a considerable difference between the sampling volumes of GPR and TDR (Huisman *et al.*, 2001; Klotzsche *et al.*, 2019), which likely explains a considerable part of the observed scatter given the lateral heterogeneity of soil within the 7-m long facility.

To independently validate the GPR and TDR results, the change in water storage of the total profile was calculated for each individual measurement time (Fig. 11). To do so, the initial water storage before the start of the first infiltration experiment was subtracted from all other water storages calculated from the estimated SWC (Loeffler and Bano, 2004). Therefore, the increase in soil water storage for the upper 1.3 m depth can be directly compared with the total amount of irrigated water. The standard deviation of the SWC measurements obtained with GPR was used to represent the spatial variation of the water storage along the borehole tubes (black error bars in Fig. 11). Also, the spatial variation of the TDR water storage along the facility wall was visualized (yellow error bars in Fig. 11). It can be seen that the observed TDR water storage systematically overestimated the expected increase in water storage based on the irrigation amount by around 25% for day 1 to day 3. On the contrary, the increase in water storage obtained from borehole GPR only showed a 5–10% underestimation for day 1 and day 2. This is attributed to the lack of information on the SWC up to a depth of 0.2 m. By combining the surface and borehole GPR data, the error in water storage estimates was further reduced to 4–8% for day 1, 2, and 4. Only for day 3, the combined GPR results overestimated the increase in water storage by 8 mm (10%), which can be explained by the relatively large uncertainty in the time-zero estimation for borehole GPR measurements at day 3 (Fig. 5). Towards the end of the infiltration experiment, it is likely that water drained below the investigated depth range due to deep drainage (Fig. 8). Therefore, an underestimation of the increase in water storage should be expected for day 3 and day 4. Although the combined GPR result showed a good match with the known water amount for day 4, the water storage of the field is thus still potentially overestimated. Overall, it is concluded that the combined borehole and surface GPR measurements outperformed the two other methods for water storage estimation in this study.
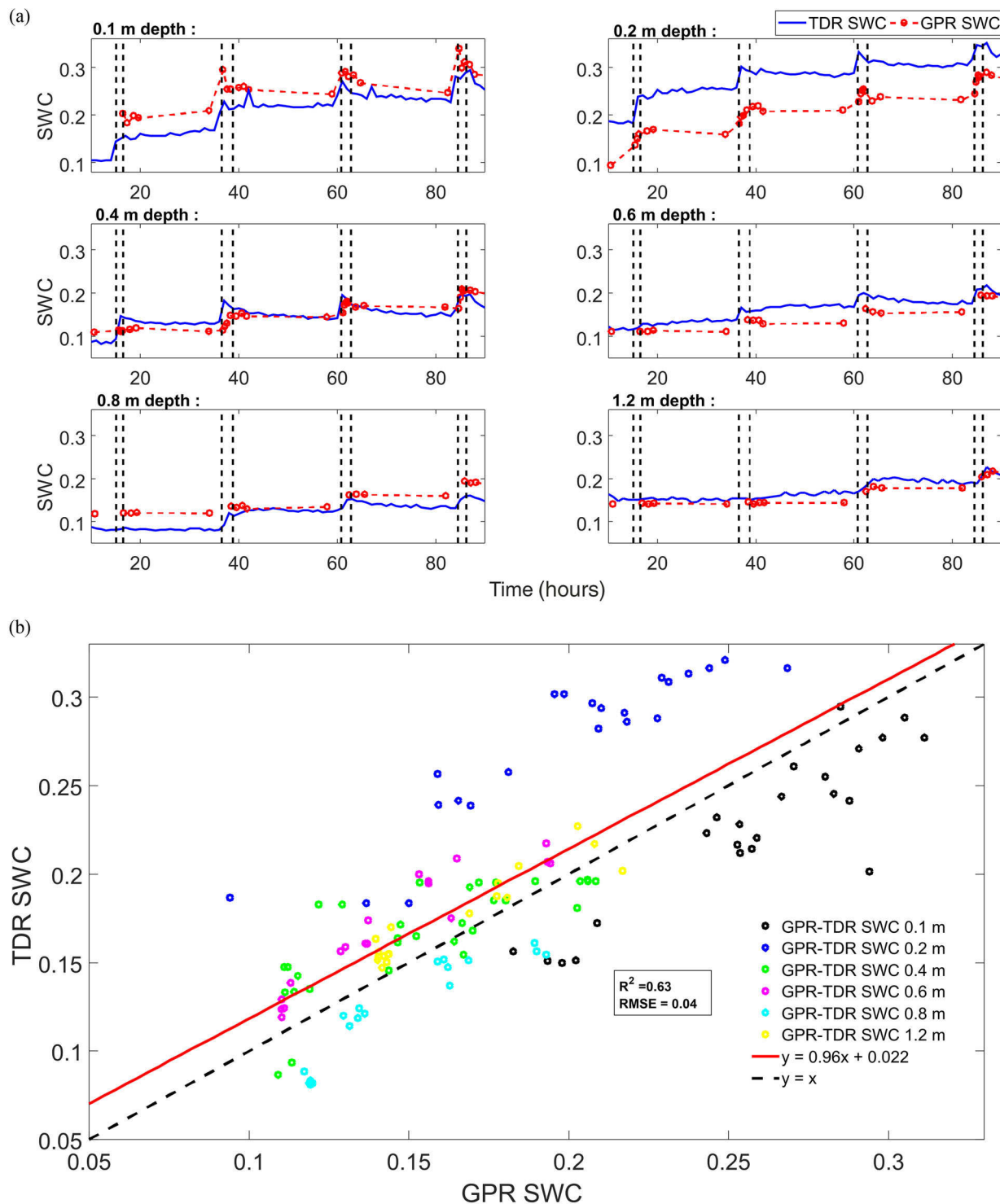
Figure 10 (a) SWC time series at different depths obtained with GPR and TDR. Black dashed lines indicate the start and end time of infiltration events. (b) Comparison of SWC measurements obtained with GPR and TDR. Different colours represent different depths of investigation. Both the 1:1 line (dashed black) and a linear regression (red) are also shown.
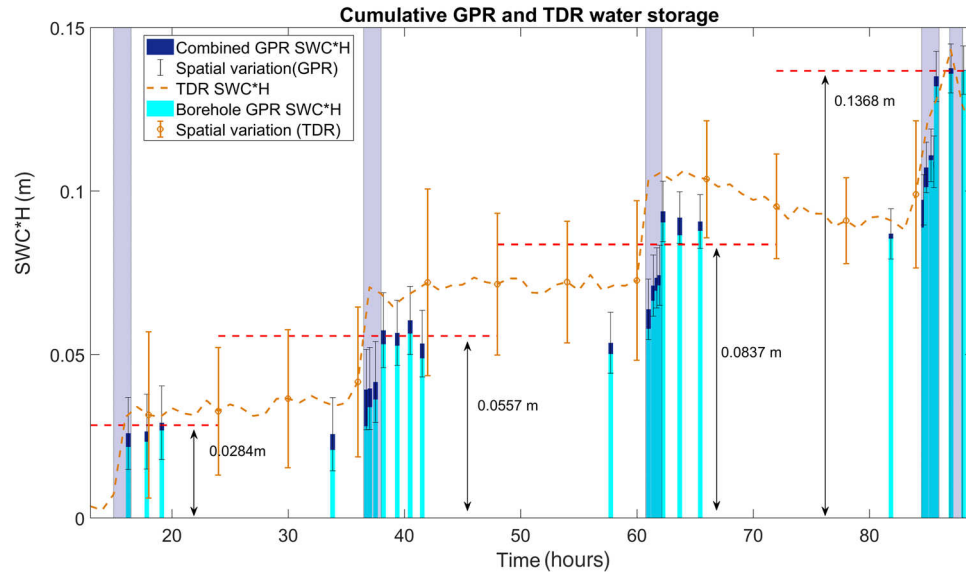
Figure 11 Time series of changes in water storage estimated with borehole GPR (light blue bars), a combination of borehole and surface GPR (dark blue bars), and TDR (yellow dashed line). Light purple bar indicate time of irrigation and red dotted line the total water added to the system.

SUMMARY AND CONCLUSION

In this study, surface and horizontal borehole ground penetrating radar (GPR) measurements were combined to investigate soil water content (SWC) dynamics up to a depth of 1.2 m in a field-scale infiltration experiment. Borehole GPR measurements provided SWC at five depths using zero-offset profiling (ZOP) surveys. Reference time domain reflectometry (TDR) measurements were taken hourly at six depths. In general, wetting front movement over the experimental period could clearly be monitored using GPR and TDR. However, the use of horizontal borehole GPR data alone failed to provide information on SWC changes of the top soil since the interpretation of borehole GPR measurements at 0.1 m depth was hindered by the interference of direct and critically refracted waves. Therefore, we additionally made surface GPR measurements to characterize the top soil. The surface GPR measurements with 500 MHz antenna showed infiltration-induced waveguides. Single-layer waveguide inversion was used to invert waveguide properties. By combining surface and horizontal borehole GPR results, representative vertical SWC profiles over the entire depth (0–1.2 m) were obtained for the entire infiltration experiment. The SWC profiles obtained by borehole GPR, combined borehole/surface GPR and TDR were used to calculate water storage changes after infiltration and were compared to the amount of irrigated water. This analysis showed that TDR systematically overestimated the increase in water storage,

which was attributed to the poor spatial representativeness of the local TDR measurements. The increase in water storage due to infiltration calculated from borehole GPR only underestimated water storage as long as the topsoil layer was not saturated. The combined use of borehole and surface GPR measurements provided the most accurate estimates of the increase in water storage. Nevertheless, further studies are needed to prove the advantage of the combined borehole/surface method for more natural infiltration events (e.g. natural rainfall). In addition, future work will explore the use of coupled hydrogeophysical inversion approaches to estimate soil hydraulic properties from the GPR data.

DATA AVAILABILITY STATEMENT

I confirm that my article contains a Data Availability Statement even if no data is available unless my article type does not require one. I confirm that I have included a citation for available data in my references section, unless my article type is exempt.

ORCID

Yi Yu https://orcid.org/0000-0001-6104-3010
Anja Klotzsche https://orcid.org/0000-0002-7021-5045
Lutz Weihermüller
https://orcid.org/0000-0003-1991-7735
Johan Alexander Huisman
https://orcid.org/0000-0002-1327-0945
Jan Vanderborght
https://orcid.org/0000-0001-7381-3211
Harry Vereecken https://orcid.org/0000-0002-8051-8517
Jan van der Kruk https://orcid.org/0000-0003-2348-1436

REFERENCES

Allroggen, N., van Schaik, N.L.M.B. and Tronicke, J. (2015) 4D ground-penetrating radar during a plot scale dye tracer experiment. *Journal of Applied Geophysics*, 118, 139–144. https://doi.org/10.1016/j.jappgeo.2015.04.016.

Arcone, S.A. (1984) Field observations of electromagnetic pulse propagation in dielectric slabs. *Geophysics*, 49(10), 1763–1773. https://doi.org/10.1190/1.1441584.

Arcone, S.A., Peapples, P.R. and Liu, L. (2003) Propagation of a ground-penetrating radar (GPR) pulse in a thin-surface waveguide. *Geophysics*, 68(6), 1922–1933. https://doi.org/10.1190/1.1635046.

Bikowski, J., Huisman, J.A., Vrugt, J.A., Vereecken, H. and Kruk, J.v.d. (2012) Integrated analysis of waveguide dispersed GPR pulses using deterministic and Bayesian inversion methods. *Near Surface Geophysics*, 10(6), 641–652. https://doi.org/10.3997/1873-0604.2012041.

Binley, A., Hubbard, S.S., Huisman, J.A., Revil, A., Robinson, D.A., Singha, K. *et al.* (2015) The emergence of hydrogeophysics for improved understanding of subsurface processes over multiple scales. *Water Resources Research*, 51(6), 3837–3866. https://doi.org/10.1002/2015wr017016.

Binley, A., Winship, P., Middleton, R., Pokar, M. and West, J. (2001) High-resolution characterization of vadose zone dynamics using cross-borehole radar. *Water Resources Research*, 37(11), 2639–2652. https://doi.org/10.1029/2000wr000089.

Busch, S., Weihermüller, L., Huisman, J.A., Steelman, C.M., Endres, A.L., Vereecken, H. and van der Kruk, J. (2013) Coupled hydrogeophysical inversion of time-lapse surface GPR data to estimate hydraulic properties of a layered subsurface. *Water Resources Research*, 49(12), 8480–8494. https://doi.org/10.1002/2013WR013992.

Cai, G., Vanderborght, J., Couvreur, V., Mboh, C.M. and Vereecken, H. (2018b) Parameterization of root water uptake models considering dynamic root distributions and water uptake compensation. *Vadose Zone Journal*, 17(1), 1–21. https://doi.org/10.2136/vzj2016.12.0125.

Cai, G., Vanderborght, J., Klotzsche, A., van der Kruk, J., Neumann, J., Hermes, N. *et al.* (2016) Construction of minirhizotron facilities for investigating root zone processes. *Vadose Zone Journal*, 15(9), vzj2016.05.0043. https://doi.org/10.2136/vzj2016.05.0043.

Cai, G., Vanderborght, J., Langensiepen, M., Schnepf, A., Hüging, H. and Vereecken, H. (2018a) Root growth, water uptake, and sap flow of winter wheat in response to different soil water conditions. *Hydrology and Earth System Sciences*, 22(4), 2449–2470. https://doi.org/10.5194/hess-22-2449-2018.

Cassiani, G., Giustiniani, M., Ferraris, S., Deiana, R. and Strobbia, C. (2009) Time-lapse surface-to-surface GPR measurements to monitor a controlled infiltration experiment. *Bollettino di Geofisica Teorica ed Applicata*, 50, 209–226.

Dafflon, B., Irving, J. and Barrash, W. (2011) Inversion of multiple intersecting high-resolution crosshole GPR profiles for hydrological characterization at the Boise Hydrogeophysical Research Site. *Journal of Applied Geophysics*, 73(4), 305–314. https://doi.org/10.1016/j.jappgeo.2011.02.001.

Dal Bo, I., Klotzsche, A., Schaller, M., Ehlers, T.A., Kaufmann, M.S., Fuentes Espoz, J.P., Vereecken, H. and van der Kruk, J. (2019) Geophysical imaging of regolith in landscapes along a climate and vegetation gradient in the Chilean coastal cordillera. *Catena*, 180, 146–159. https://doi.org/10.1016/j.catena.2019.04.023.

Doetsch, J., Linde, N., Coscia, I., Greenhalgh, S.A. and Green, A.G. (2010) Zonation for 3D aquifer characterization based on joint inversions of multimethod crosshole geophysical data. *Geophysics*, 75(6), G53–G64. https://doi.org/10.1190/1.3496476.

Galagedara, L.W., Parkin, G.W. and Redman, J.D. (2005b) Measuring and modeling of direct ground wave depth penetration under transient soil moisture conditions. *Subsurface Sensing Technologies and Applications*, 6(2), 193–205. https://doi.org/10.1007/s11220-005-0006-z.

Galagedara, L.W., Parkin, G.W., Redman, J.D. and Endres, A.L. (2002) Temporal and spatial variation of soil water content measured by borehole GPR under irrigation and drainage. Proc. SPIE 4758, 180–185. Ninth International Conference of Ground Penetrating Radar (GPR 2002). https://doi.org/10.1117/12.462253.

Galagedara, L.W., Redman, J.D., Parkin, G.W., Annan, A.P. and Endres, A.L. (2005a) Numerical modeling of GPR to determine the direct ground wave sampling depth. *Vadose Zone Journal*, 4(4), 1096–1106. https://doi.org/10.2136/vzj2004.0143.

Giannopoulos, A. (2005) Modelling ground penetrating radar by GprMax. *Construction and Building Materials*, 19(10), 755–762. https://doi.org/10.1016/j.conbuildmat.2005.06.007.

Grote, K., Anger, C., Kelly, B., Hubbard, S. and Rubin, Y. (2010) Characterization of soil water content variability and soil texture using GPR groundwave techniques. *Journal of Environmental and Engineering Geophysics*, 15(3), 93–110. https://doi.org/10.2113/JEEG15.3.93.

Grote, K., Hubbard, S. and Rubin, Y. (2003) Field-scale estimation of volumetric water content using ground-penetrating radar

ground wave techniques. *Water Resources Research*, 39(11), 5–13. https://doi.org/10.1029/2003wr002045.

Holliger, K., Musil, M. and Maurer, H.R. (2001) Ray-based amplitude tomography for crosshole georadar data: a numerical assessment. *Journal of Applied Geophysics*, 47(3), 285–298. https://doi.org/10.1016/S0926-9851(01)00072-6.

Huisman, J.A., Hubbard, S.S., Redman, J.D. and Annan, A.P. (2003b) Measuring soil water content with ground penetrating radar: a review. *Vadose Zone Journal*, 2(4), 476–491. https://doi.org/10.2113/2.4.476.

Huisman, J.A., Snepvangers, J.J.J.C., Bouten, W. and Heuvelink, G.B.M. (2002) Mapping spatial variation in surface soil water content: comparison of ground-penetrating radar and time domain reflectometry. *Journal of Hydrology*, 269(3), 194–207. https://doi.org/10.1016/S0022-1694(02)00239-1.

Huisman, J.A., Snepvangers, J.J.J.C., Bouten, W. and Heuvelink, G.B.M. (2003a) Monitoring temporal development of spatial soil water content variation: comparison of ground penetrating radar and time domain reflectometry. *Vadose Zone Journal*, 2(4), 519–529. https://edepot.wur.nl/351324.

Huisman, J.A., Sperl, C., Bouten, W. and Verstraten, J.M. (2001) Soil water content measurements at different scales: accuracy of time domain reflectometry and ground-penetrating radar. *Journal of Hydrology*, 245(1), 48–58. https://doi.org/10.1016/S0022-1694(01)00336-5.

Iwasaki, T., Kuroda, S., Saito, H., Tobe, Y., Suzuki, K., Fujimaki, H. and Inoue, M. (2016) Monitoring infiltration process seamlessly using array ground penetrating radar. *Agricultural & Environmental Letters*, 1(1), 1–4. https://doi.org/10.2134/ael2016.01.0002.

Jadoon, K.Z., Weihermüller, L., Scharnagl, B., Kowalsky, M.B., Bechtold, M., Hubbard, S.S. *et al.* (2012) Estimation of soil hydraulic parameters in the field by integrated hydrogeophysical inversion of time-lapse ground-penetrating radar data. *Vadose Zone Journal*, 11(4), vzj2011.0177. https://doi.org/10.2136/vzj2011.0177.

Jaumann, S. and Roth, K. (2018) Soil hydraulic material properties and layered architecture from time-lapse GPR. *Hydrology and Earth System Sciences*, 22(4), 2551–2573. https://doi.org/10.5194/hess-22-2551-2018.

Kelter, M., Huisman, J.A., Zimmermann, E. and Vereecken, H. (2018) Field evaluation of broadband spectral electrical imaging for soil and aquifer characterization. *Journal of Applied Geophysics*, 159, 484–496. https://doi.org/10.1016/j.jappgeo.2018.09.029.

Klotzsche, A., Jonard, F., Looms, M.C., van der Kruk, J. and Huisman, J.A. (2018) Measuring soil water content with ground penetrating radar: a decade of progress. *Vadose Zone Journal*, 17(1), 1–9. https://doi.org/10.2136/vzj2018.03.0052.

Klotzsche, A., Lärm, L., Vanderborght, J., Cai, G., Morandage, S., Zörner, M. *et al.* (2019) Monitoring soil water content using time-lapse horizontal borehole GPR data at the field-plot scale. *Vadose Zone Journal* 18, 190044. https://doi.org/10.2136/vzj2019.05.0044

Klotzsche, A., van der Kruk, J., Linde, N., Doetsch, J. and Vereecken, H. (2013) 3-D characterization of high-permeability zones in a gravel aquifer using 2-D crosshole GPR full-waveform inversion and waveguide detection. *Geophysical Journal International*, 195(2), 932–944. https://doi.org/10.1093/gji/ggt275.

Knight, R. (2001) Ground penetrating radar for environmental applications. *Annual Review of Earth and Planetary Sciences*, 29(1), 229–255. https://doi.org/10.1146/annurev.earth.29.1.229

Loeffler, O. and Bano, M. (2004) Ground penetrating radar measurements in a controlled vadose zone. *Vadose Zone Journal* 3, 1082. https://doi.org/10.2136/vzj2004.1082.

Lunt, I.A., Hubbard, S.S. and Rubin, Y. (2005) Soil moisture content estimation using ground-penetrating radar reflection data. *Journal of Hydrology*, 307(1), 254–269. https://doi.org/10.1016/j.jhydrol.2004.10.014.

Mangel, A.R., Moysey, S.M.J. and van der Kruk, J. (2015) Resolving precipitation induced water content profiles by inversion of dispersive GPR data: a numerical study. *Journal of Hydrology*, 525, 496–505. https://doi.org/10.1016/j.jhydrol.2015.04.011.

Mangel, A.R., Moysey, S.M.J. and van der Kruk, J. (2017) Resolving infiltration-induced water content profiles by inversion of dispersive ground-penetrating radar data. *Vadose Zone Journal*, 16(10), 1–11. https://doi.org/10.2136/vzj2017.02.0037.

Mangel, A.R., Moysey, S.M.J., Ryan, J.C. and Tarbutton, J.A. (2012) Multi-offset ground-penetrating radar imaging of a lab-scale infiltration test. *Hydrology and Earth System Sciences*, 16(11), 4009–4022. https://doi.org/10.5194/hess-16-4009-2012.

Pan, X., Zhang, J., Huang, P. and Roth, K. (2012) Estimating field-scale soil water dynamics at a heterogeneous site using multi-channel GPR. *Hydrology and Earth System Sciences*, 16(11), 4361–4372. https://doi.org/10.5194/hess-16-4361-2012.

Park, C.B., Miller, R.D. and Xia, J. (1998) Imaging dispersion curves of surface waves on multi-channel record. SEG Technical Program Expanded Abstracts 1998: Society of Exploration Geophysicists SEG Technical Program Expanded Abstracts, 1377–1380.

Peterson, J.E., Jr. (2001) Pre-inversion corrections and analysis of radar tomographic data. *Journal of Environmental and Engineering Geophysics*, 6(1), 1–18. https://doi.org/10.4133/jeeg6.1.1.

Rejiba, F., Sagnard, F., Schamper, C., Froumentin, M. and Guerin, R. (2011) Zero-offset profiling using frequency cross-hole radars in a layered embankment test site: antenna design, simulation and experimental results. *Near Surface Geophysics* 9, 67–76. https://doi.org/10.3997/1873-0604.2010058

Redman, D., Parkin, G.W. and Annan, A.P. (2000) Borehole GPR measurement of soil water content during an infiltration experiment. Proceedings of SPIE Vol. 4084, 8th International Conference on Ground Penetrating Radar.

Rossi, M., Manoli, G., Pasetto, D., Deiana, R., Ferraris, S., Strobbia, C. *et al.* (2015) Coupled inverse modeling of a controlled irrigation experiment using multiple hydro-geophysical data. *Advances in Water Resources*, 82, 150–165. https://doi.org/10.1016/j.advwatres.2015.03.008.

Roth, K., Schulin, R., Flühler, H. and Attinger, W. (1990) Calibration of time domain reflectometry for water content measurement using a composite dielectric approach. *Water Resources Research*, 26(10), 2267–2273. https://doi.org/10.1029/WR026i010p02267.

Slob, E., Sato, M. and Olhoeft, G. (2010) Surface and borehole ground-penetrating-radar developments. *Geophysics*, 75(5), 75A103-175A120. https://doi.org/10.1190/1.3480619.

Steelman, C.M., Endres, A.L. and Jones, J.P. (2012) High-resolution ground-penetrating radar monitoring of soil moisture dynamics:

Field results, interpretation, and comparison with unsaturated flow model. *Water Resources Research*, 48(9), W09538. https://doi.org/10.1029/2011wr011414.

Strobbia, C. and Cassiani, G. (2007) Multilayer ground-penetrating radar guided waves in shallow soil layers for estimating soil water content. *Geophysics*, 72(4), J17–J29. https://doi.org/10.1190/1.2716374.

van der Kruk, J. (2006) Properties of surface waveguides derived from inversion of fundamental and higher mode dispersive GPR data. *IEEE Transactions on Geoscience and Remote Sensing*, 44(10), 2908–2915. https://doi.org/10.1109/TGRS.2006.877286.

van der Kruk, J., Jacob, R.W. and Vereecken, H. (2010) Properties of precipitation-induced multilayer surface waveguides derived from inversion of dispersive TE and TM GPR data. *Geophysics*, 75(4), WA263-WA273. https://doi.org/10.1190/1.3467444.

van der Kruk, J., Streich, R. and Green, A.G. (2006) Properties of surface waveguides derived from separate and joint inversion of dispersive TE and TM GPR data. *Geophysics*, 71(1), K19–K29. https://doi.org/10.1190/1.2168011.

van der Kruk, J., Steelman, C.M., Endres, A.L. and Vereecken, H. (2009) Dispersion inversion of electromagnetic pulse propagation within freezing and thawing soil waveguides. *Geophysical Research Letters*, 36(18), L18503. https://doi.org/10.1029/2009gl039581.

van Overmeeren, R.A., Sariowan, S.V. and Gehrels, J.C. (1997) Ground penetrating radar for determining volumetric soil water content; results of comparative measurements at two test sites. *Journal of Hydrology*, 197(1), 316–338. https://doi.org/10.1016/S0022-1694(96)03244-1.

Warren, C., Giannopoulos, A. and Giannakis, I. (2016) gprMax: open source software to simulate electromagnetic wave propagation for Ground Penetrating Radar. *Computer Physics Communications*, 209, 163–170. https://doi.org/10.1016/j.cpc.2016.08.020.

Weihermüller, L., Huisman, J.A., Hermes, N., Pickel, S. and Vereecken, H. (2013) A new TDR multiplexing system for reliable electrical conductivity and soil water content measurements. *Vadose Zone Journal*, 12, 1–11. https://doi.org/10.2136/vzj2012.0194.

Weihermüller, L., Huisman, J.A., Lambot, S., Herbst, M. and Vereecken, H. (2007) Mapping the spatial variation of soil water content at the field scale with different ground penetrating radar techniques. *Journal of Hydrology*, 340(3), 205–216. https://doi.org/10.1016/j.jhydrol.2007.04.013.

Yang, X., Klotzsche, A., Meles, G., Vereecken, H. and van der Kruk, J. (2013) Improvements in crosshole GPR full-waveform inversion and application on data measured at the Boise Hydrogeophysics Research Site. *Journal of Applied Geophysics*, 99, 114–124. https://doi.org/10.1016/j.jappgeo.2013.08.007.